Defective fluid shear stress mechanotransduction mediates hereditary hemorrhagic telangiectasia

Nicolas Baeyens,[1,2*] Bruno Larrivée,[1,2,3*] Roxana Ola,[1,2] Brielle Hayward-Piatkowskyi,[1,2] Alexandre Dubrac,[1,2] Billy Huang,[1,2] Tyler D. Ross,[1,2] Brian G. Coon,[1,2] Elizabeth Min,[1,2] Maya Tsarfati,[1,2] Haibin Tong,[1,2,4] Anne Eichmann,[1,5**] and Martin A. Schwartz[1,6,7**]

[1]Department of Medicine (Cardiology), Yale University School of Medicine, New Haven, CT 06511
[2]Yale Cardiovascular Research Center, Yale University School of Medicine, New Haven, CT 06511
[3]Department of Ophthalmology, Maisonneuve-Rosemont Hospital Research Centre, University of Montreal, Montreal, Quebec H3T 1J4, Canada
[4]Jilin Provincial Key Laboratory of Molecular Geriatric Medicine, Life Science Research Center, Beihua University, Jilin 132013, China
[5]Institut National de la Santé et de la Recherche Médicale U970, Paris Center for Cardiovascular Research, 75015 Paris, France
[6]Department of Cell Biology and [7]Department of Biomedical Engineering, Yale University, New Haven, CT 06510

Morphogenesis of the vascular system is strongly modulated by mechanical forces from blood flow. Hereditary hemorrhagic telangiectasia (HHT) is an inherited autosomal-dominant disease in which arteriovenous malformations and telangiectasias accumulate with age. Most cases are linked to heterozygous mutations in *Alk1* or *Endoglin*, receptors for bone morphogenetic proteins (BMPs) 9 and 10. Evidence suggests that a second hit results in clonal expansion of endothelial cells to form lesions with poor mural cell coverage that spontaneously rupture and bleed. We now report that fluid shear stress potentiates BMPs to activate Alk1 signaling, which correlates with enhanced association of Alk1 and endoglin. Alk1 is required for BMP9 and flow responses, whereas endoglin is only required for enhancement by flow. This pathway mediates both inhibition of endothelial proliferation and recruitment of mural cells; thus, its loss blocks flow-induced vascular stabilization. Identification of Alk1 signaling as a convergence point for flow and soluble ligands provides a molecular mechanism for development of HHT lesions.

Introduction

Hereditary hemorrhagic telangiectasia (HHT) is an inherited autosomal-dominant disease characterized by telangiectasias that consist of clusters of small, dilated blood vessels, and by larger, high flow arteriovenous malformations (AVMs) that directly connect arteries and veins (Shovlin, 2010; Atri et al., 2014; McDonald et al., 2015). Lesions are typically fragile, leading to frequent episodes of bleeding, most often in the lining of the nose and the gastrointestinal tract, but also the lung, brain and liver. Abundant high flow AVMs can also cause cardiac insufficiency. HHT lesions tend to appear later in life, with recurrent nosebleeds (epistaxis), beginning on average around age 12 and GI bleeding appearing most commonly after age 50.

Approximately 85% of HHT cases are associated with heterozygous mutations in activin receptor-like kinase1 (*ACVRL1* or *Alk1*; type 2 HHT) or its coreceptor, *Endoglin* (*ENG*; type I HHT), and an additional 4% are linked to mutations in their downstream effector *Smad4* (McDonald et al., 2015). Alk1 is a type I receptor for the bone morphogenetic protein (BMP) family proteins BMP9 and BMP10 (Tillet and Bailly, 2015). BMP9, which is a circulating factor produced by the liver, signals through Alk1 in endothelial cells (ECs) to inhibit angiogenesis in a context-specific manner (David et al., 2007, 2008). Alk1 activation by its ligands induces association with BMP type 2 receptors and downstream phosphorylation of Smad1/5/8 transcription factors, which in turn regulate gene expression. The late and focal appearance of HHT lesions is likely related to the need for a so-called second hit to inactivate the normal allele and/or other related pathways.

Embryonic deletion of *Acvrl1* or *Eng* in mice leads to lethality in midgestation with grossly defective vasculature (Arthur et al., 2000; Oh et al., 2000; Sorensen et al., 2003). Heterozygous mutations in either gene give rise to lesions similar

*N. Baeyens and B. Larrivée contributed equally to this paper.

**A. Eichmann and M.A. Schwartz contributed equally to this paper.

Correspondence to Martin A. Schwartz: martin.schwartz@yale.edu

N. Baeyens' present address is Wellcome Trust Centre for Cell-Matrix Research, The University of Manchester, Manchester M13 9PL, England, UK.

T.D. Ross' present address is Center for Systems and Synthetic Biology and Department of Biochemistry and Biophysics, California Institute for Quantitative Biosciences, University of California, San Francisco, San Francisco, CA 94143.

Abbreviations used: ANOVA, analysis of variance; AVM, arteriovenous malformation; EC, endothelial cell; EC_{50}, half maximal effective concentration; FSS, fluid shear stress; HHT, hereditary hemorrhagic telangiectasia; HUVEC, human umbilical vein endothelial cell; P, postnatal day; VEGFR, vascular endothelial growth factor receptor.

The Rockefeller University Press $30.00
J. Cell Biol. Vol. 214 No. 7 807–816
www.jcb.org/cgi/doi/10.1083/jcb.201603106

to human HHT, but these lesions form at low frequency and with very long latency, typically in mice >1 yr of age, making it an inconvenient model. Inducible homozygous deletion of either gene in postnatal or adult mice gives rise to lesions that resemble those formed in human disease, including AVMs with poor smooth muscle coverage and hemorrhage (Tual-Chalot et al., 2015). Interestingly, microenvironmental factors also play an important role, as even after homozygous genetic deletions, lesions form preferentially when combined with local angiogenic or proinflammatory stimuli (Park et al., 2009; Garrido-Martin et al., 2014).

Biomechanical forces, which play a critical role in shaping the vascular system to optimize perfusion (Baeyens and Schwartz, 2016), have recently been shown to participate in the development of HHT lesions such as AVMs. *Alk1* loss-of-function mutations in zebrafish lead to pathological arterial enlargement, resulting in altered blood flow (Corti et al., 2011). Downstream vessels adapted to consequent increases in flow by retaining normally transient arteriovenous drainage connections that enlarge into AVMs. These authors proposed that effects were mediated by a combination of flow induction of Alk1 expression and delivery of its ligand, BMP10, through the bloodstream (Laux et al., 2013). Smads 1/5/8 have also been reported to be activated by fluid flow (Zhou et al., 2012), though the receptors and upstream mechanisms were not investigated. These considerations led us to evaluate the contribution of shear stress on Alk1 and endoglin signaling as well as their role in EC responses to shear stress. Our results show that mechanical forces induce Alk1 interaction with endoglin and potentiate the activity of BMP9 by lowering its half maximal effective concentration (EC_{50}) and that activation of endoglin and Alk1 under shear stress mediates vascular quiescence by inhibiting EC proliferation and promoting pericyte recruitment.

Results and discussion

Loss of Alk1 results in the formation of arteriovenous shunts in the presence of flow

The retinal vasculature develops after birth with the sprouting of a vascular network that starts at the optic nerve and progressively covers the whole retina. The network quickly differentiates into mature arteries and veins interconnected by a capillary network. Computational analysis of blood velocities and shear stress distribution within this developing network revealed a gradient with high shear stress close to the optic nerve and decreasing toward the sprouting front (Bernabeu et al., 2014). To determine whether blood flow plays a role in AVM development in response to impaired Alk1 signaling, we induced endothelial *Alk1* deletion during postnatal retinal angiogenesis by crossing *Alk1*$^{l/l}$ and *Cdh5-CreERT2* mice (*Alk1*^{iEC}; Aspalter et al., 2015). When *Alk1* was deleted at postnatal day 3 (P3), it produced arteriovenous shunts by day 5 (Fig. 1 A), similar to the observations of Tual-Chalot et al. (2014). Interestingly, we observed that the shunts were only formed close to the optic nerve, within the better-differentiated vascular plexus, where blood flow was high (Fig. 1 B). In the sprouting front, where blood flow is lower, we instead observed increased branching and hypersprouting, which was never observed in the well-perfused vascular plexus (Fig. 1, A and C). A similar phenotype was observed after intraperitoneal injection of blocking antibodies against BMP9 and BMP10 at P3 (Fig. 1, D–F). When AVM formation was initiated in adult mice by Alk1 deletion and wounding, AVMs were also associated with regions of high blood flow velocity (Park et al., 2009). Thus, impaired Alk1 signaling results in the formation of vascular shunts specifically in regions of high blood flow.

Endoglin promotes shear stress activation of Alk1 signaling

These results led us to consider whether fluid shear stress (FSS) from blood flow might directly modulate Alk1 signaling. To test this idea, human umbilical vein endothelial cells (HUVECs) in low serum medium (0.2% FBS) were treated with 1 ng/ml BMP9 or subjected to FSS in the physiological range (12 dynes/cm^2), and Smad activation was assessed. FSS induced both Smad phosphorylation and nuclear translocation, with a time course that was slightly slower than soluble BMP9, though of similar magnitude (Fig. 2, A and B; and Fig. S1 A). Smad1 was most strongly affected, followed by Smad5, with little change in Smad8. We therefore focused on Smad1. To test whether these effects were mediated by the known BMP9 receptors, Alk1 and endoglin levels were reduced using siRNA. Depletion of Alk1 blocked Smad1 activation by both BMP9 and FSS, whereas depletion of endoglin only affected the response to flow (Fig. 2, B and C). To validate this observation, we analyzed the response to BMP9 over a wide range of concentrations. Depletion of endoglin had no effect at any dose (Fig. S1 B). Reexpression of siRNA-resistant proteins rescued Smad activation, indicating specificity (Fig. S1 C). Our previous work identified a junctional mechanosensory complex, comprising PECAM-1, VE-cadherin, and vascular endothelial growth factor receptors (VEGFRs), whose activation controls a number of flow responses, including PI3K activation and alignment in the direction of flow (Tzima et al., 2005; Coon et al., 2015). However, depletion of PECAM-1 or VEGFR2 only slightly altered Smad1/5/8 phosphorylation in response to flow. Thus, flow signaling through Alk1–endoglin appears to be independent of the PECAM–VE-cadherin–VEGFR complex.

Shear stress potentiates responses to soluble BMP9/BMP10

To investigate the mechanisms by which shear stress activates Smad signaling, we first addressed whether the effect of flow was independent of BMPs. FBS contains significant amounts of these factors, which would still be present at low levels in medium containing 0.2% serum. Therefore, cells were examined in serum-free medium containing 0.2% BSA and supplemented with various concentrations of BMP9. Without BMP9, flow failed to detectably activate Smad1, whereas addition of as little as 1 pg/ml BMP9 conferred sensitivity (Fig. 3 A). At high levels of BMP9, Smad signaling was activated without flow. BMP9 EC_{50} was shifted from ∼60 pg/ml without flow to ∼3.5 pg/ml with flow. Addition of BMP9 and BMP10 inhibitory antibodies to medium containing 0.2 FBS efficiently blocked the flow-dependent activation of Smad1 (Fig. 3 B), confirming the requirement for BMPs. Thus, FSS activates this pathway by potentiating responses to soluble BMP9/BMP10.

To gain further insight into the mechanism of these effects, we immunoprecipitated the BMP receptors. We used an adenoviral vector to express low levels of GFP tagged endoglin (∼10% of endogenous) in HUVECs, then treated the cells with either 1 ng/ml BMP9 or 12 dynes/cm^2 flow for 15 min. Immunoprecipitation of endoglin-GFP with a GFP trap,

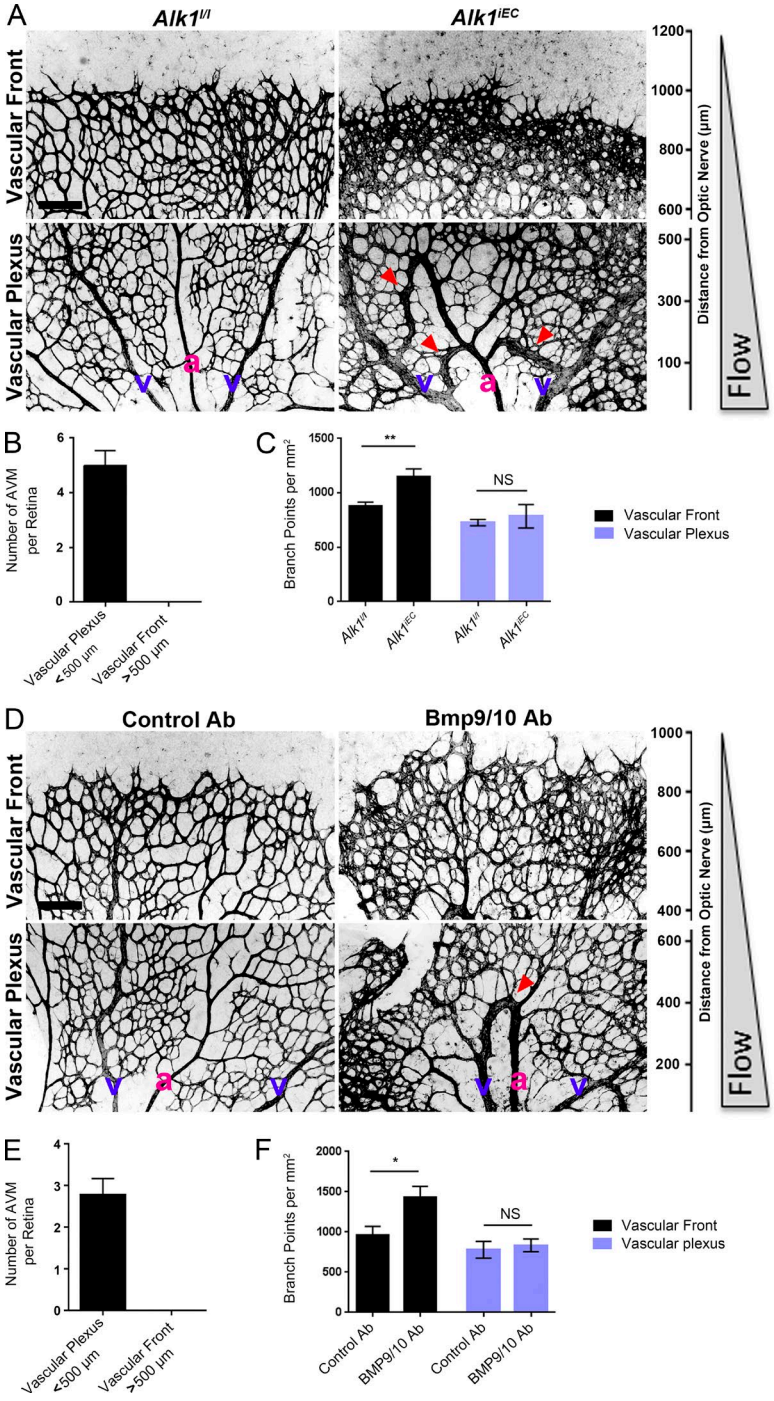

Figure 1. **Effects of blood flow on the development of retinal AVMs under impaired Alk1 signaling.** (A) Representative images of P5 retinas stained with isolectin B4 to identify blood vessels in control (*Alk1*$^{l/l}$) and *Alk1*^{iEC} (*Cdh5-CreERT2-Alk1*^{iEC}) mice after 50 µg tamoxifen injection at P3. (B) Quantification of the number of AVMs in the proximal (<500 µm from the optic nerve) versus distal (>500 µm from the optic nerve) regions of the retina ($n = 5$). (C) Quantification of the number of branch points in *Alk1*$^{l/l}$ and *Cdh5-CreERT2 (Alk1*^{iEC}) mice in the proximal versus distal regions ($n = 5$, Mann–Whitney; **, $P < 0.005$). (D) Representative images of P5 retinal vessels from pups injected at P3 with control or BMP9/BMP10 blocking antibodies. v, vein; a, artery. (E and F) Quantification of the number of AVMs (E) or branch points (F) in the proximal and distal regions in mice injected with control or BMP9/BMP10 blocking antibodies ($n = 5$, Mann–Whitney; *, $P < 0.05$). Bars, 150 µm. NS, not significant. Error bars represent SEM.

followed by immunoblotting, showed that flow induced an association between Alk1 and endoglin, whereas BMP9 alone had no effect (Fig. 3 C). These results suggest that flow and BMP9 act on these receptors in different ways, which ultimately enhances sensitivity to BMP9.

Alk1 specifically regulates flow-dependent repression of EC proliferation and pericyte recruitment

Flow within the physiological range stabilizes blood vessels primarily by inhibiting proliferation (Akimoto et al., 2000) and by inducing recruitment of mural cells (pericytes and smooth muscle cells; Van Gieson et al., 2003). AVMs have been characterized by impaired recruitment of perivascular cells and increased endothelial cell proliferation. To address the contribution of Alk1 signaling to these events, *Alk1*^{iEC} mice were crossed with mice carrying the mTmG reporter. As a new, more tractable model for HHT, these mice were then injected with a low dose of 5 µg tamoxifen to delete *Alk1* at low frequency, generating mosaic blood vessels composed initially of mainly Alk1-positive cells (mCherry) with a small number of Alk1-negative endothelial cells (GFP). Mosaic deletion of *Alk1* resulted in the formation of AVMs in the vascular plexus, which were exclusively composed of the GFP-positive cells that lack Alk1 (Fig. 4). In GFP-negative cells, proliferation was markedly decreased in the vascular plexus, but not at the vascular

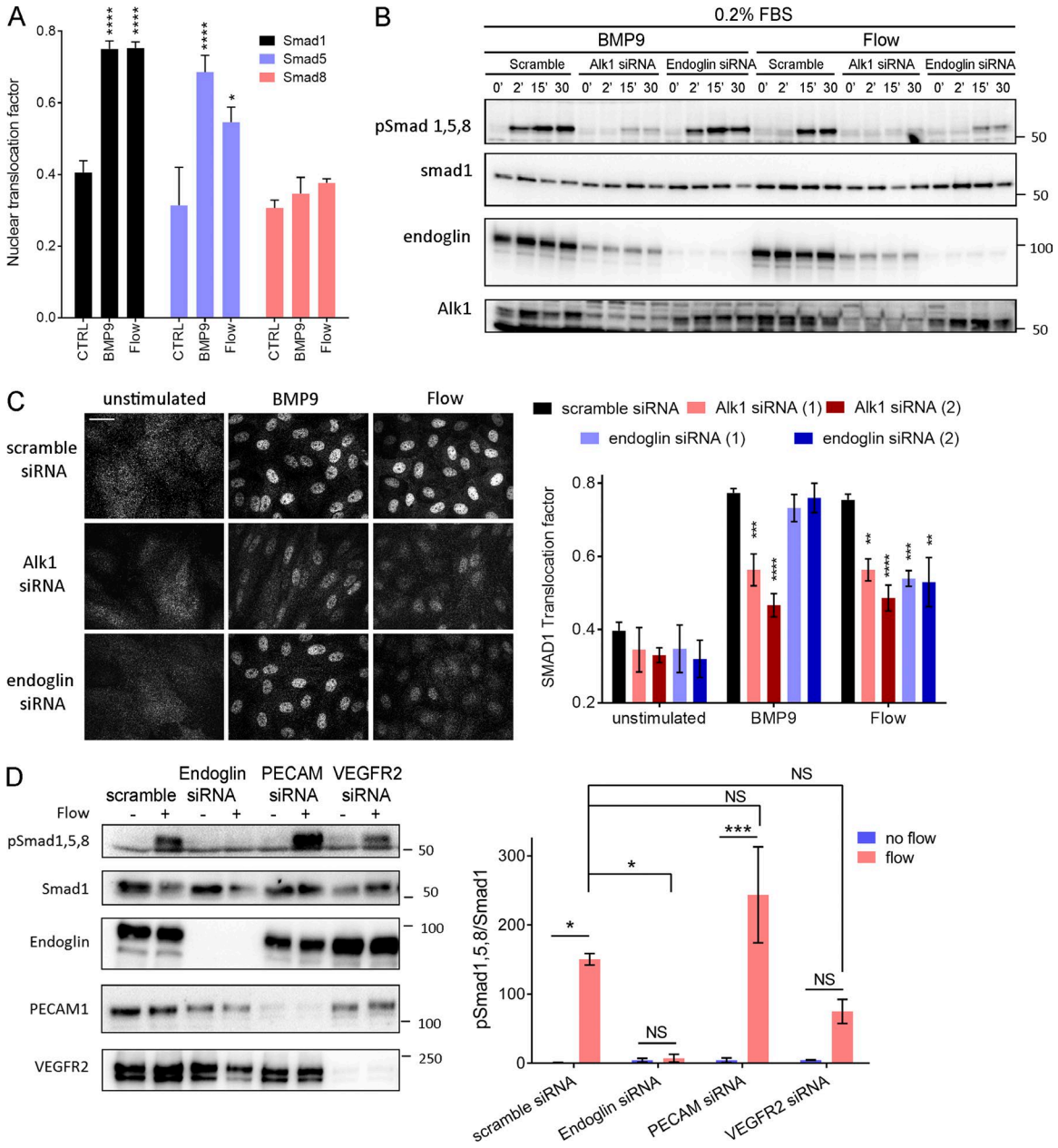

Figure 2. **Alk1 signaling in response to FSS.** (A) Nuclear translocation of Smad1, Smad5, and Smad8 in response to 1 ng/ml BMP9 or 12 dynes/cm^2 for 45 min (n = 3–8, ANOVA two-way; *, P < 0.05; ****, P < 0.0001). (B) Representative Western blots of phosphorylated Smad1,5,8, Smad1, Alk1 and endoglin in response to 1 ng/ml BMP9 or 12 dynes/cm^2 FSS for the indicated times. Actin was used as a loading control. (C) Representative staining of Smad1 in response to 1 ng/ml BMP9 or 12 dynes/cm^2 for 45 min in HUVECs transfected with the indicated siRNAs (siRNA 1: QIAGEN; siRNA 2: GE Healthcare; n = 3–11, two-way ANOVA; **, P < 0.01; ***, P < 0.001; ****, P < 0.0001). Bar, 10 µm. (D) Representative Western blot of Smad1/5/8 phosphorylation in response to 15 min of 12 dynes/cm^2 FSS in cells transfected with the indicated siRNAs (n = 3, ANOVA; *, P < 0.05; ***, P < 0.001). NS, not significant.

front, consistent with an antiproliferative role of shear stress. Strikingly, proliferation of GFP-positive cells was minimally decreased in plexus, where flow is high (Fig. 4 A). Furthermore, pericyte coverage was significantly decreased in the vascular plexus, where arteriovenous shunts form, but was unaffected in the sprouting front (Fig. 4 B). No differences in pericyte coverage were observed between recombined and unrecombined cells in control mosaic mice (Fig. S2).

As controls, we measured levels of Klf2 and Klf4 mRNA (Fig. 5 A), two transcription factors whose expression shows strong, magnitude-dependent induction by FSS in endothelial cells (Dekker et al., 2002; Hamik et al., 2007). Depletion of Alk1 or endoglin moderately increased induction of Klf2 and Klf4 by FSS. This major flow pathway therefore does not require, but instead appears to be partially restrained by, Alk1–endoglin signaling.

The respective contributions of Alk1 and endoglin in flow-mediated modulation of EC proliferation and pericyte recruitment were then evaluated. Both BMP9 and FSS strongly inhibited cell cycle progression in control cells, as expected (Fig. 5 B). Depletion of Alk1 blocked both responses; surprisingly, depletion of endoglin had no effect on cell cycle

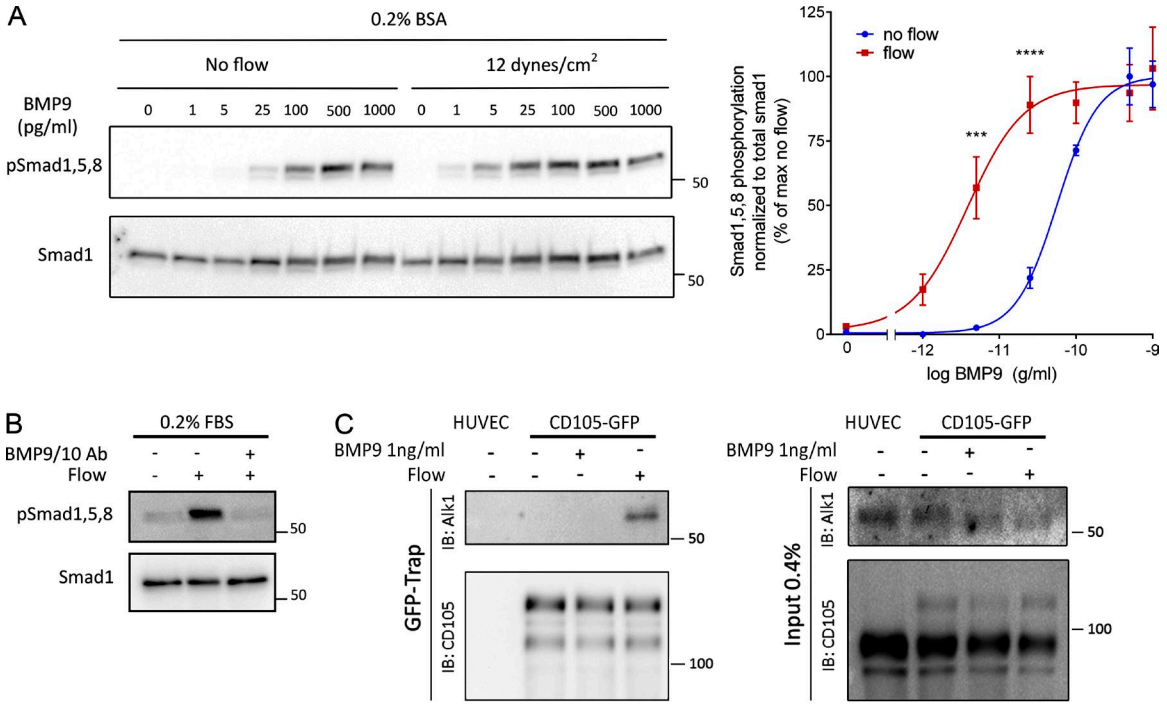

Figure 3. **Potentiation of BMP9 responses by FSS.** (A) Representative Western blot of Smad1/5/8 phosphorylation in response to the indicated concentrations of BMP9 in serum-free media with or without flow for 45 min ($n = 4$, two-way ANOVA; ***, $P < 0.001$; ****, $P < 0.0001$, BMP9 EC_{50}: 56 pg/ml without flow, 3.6 pg/ml with flow). (B) Representative Western blot of Smad1/5/8 phosphorylation in response to 12 dynes/cm^2 for 45 min in the presence or absence of two blocking antibodies against BMP9 and BMP10 (each at 100 ng/ml). (C) Association of endoglin-GFP with endogenous Alk1 in response to 1 ng/ml BMP9 or 12 dynes/cm^2 flow for 15 min. GFP-tagged proteins were captured with a GFP-trap and immunoprecipitations analyzed by immunoblotting (IB) as indicated.

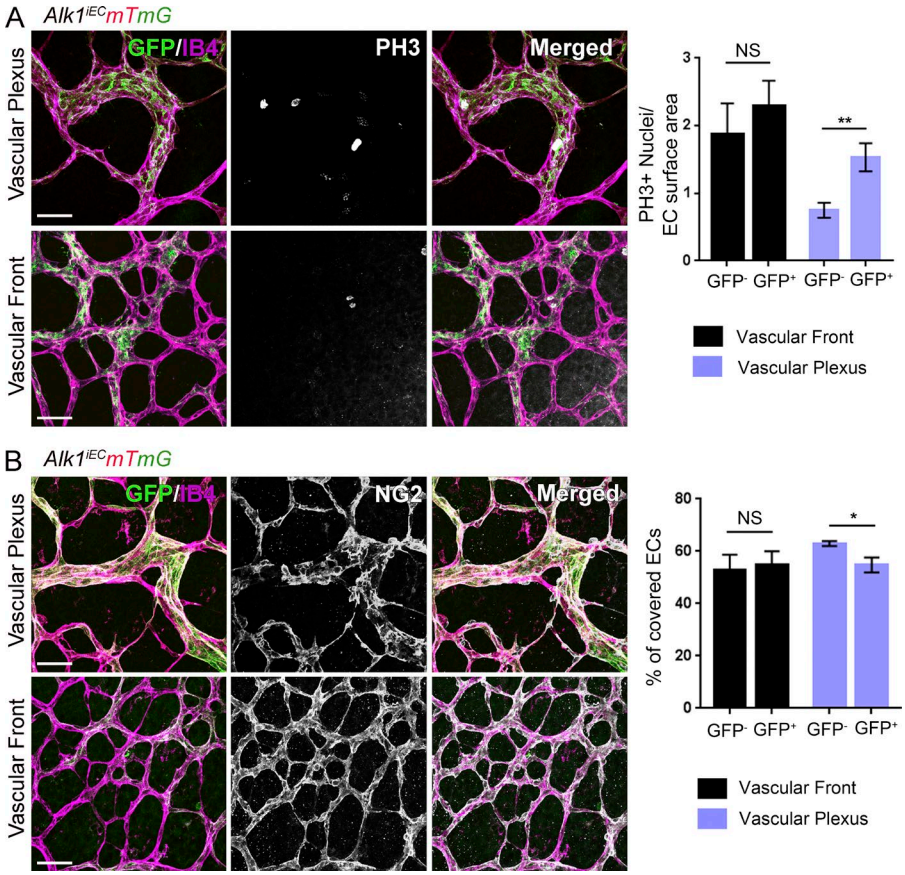

Figure 4. **Effects of Alk1 mosaic deletion on proliferation and pericyte coverage in retinal ECs.** (A) Phospho–histone H3 (PH3) staining of P6 retinas of *Cdh5-CreERT2 Alk1^{iEC}:mTmG* mice injected with low-dose (5 µg) tamoxifen at P3. Unrecombined ECs (GFP–; Alk1 positive) are shown in light purple, and recombined ECs (GFP+; Alk1 negative) are shown in green. The graph shows quantification of PH3-positive cells at the vascular front and vascular plexus in GFP– and GFP+ cells (number of positive nuclei normalized to EC surface area; $n = 6$ retinas, Mann–Whitney; **, $P < 0.005$). (B) NG2 staining of P6 retinas after *Alk1* mosaic deletion. Graph shows the percentage of EC surface area covered by NG2-positive cells ($n = 6$ retinas, Mann–Whitney; *, $P < 0.05$). Bars, 50 µm. NS, not significant.

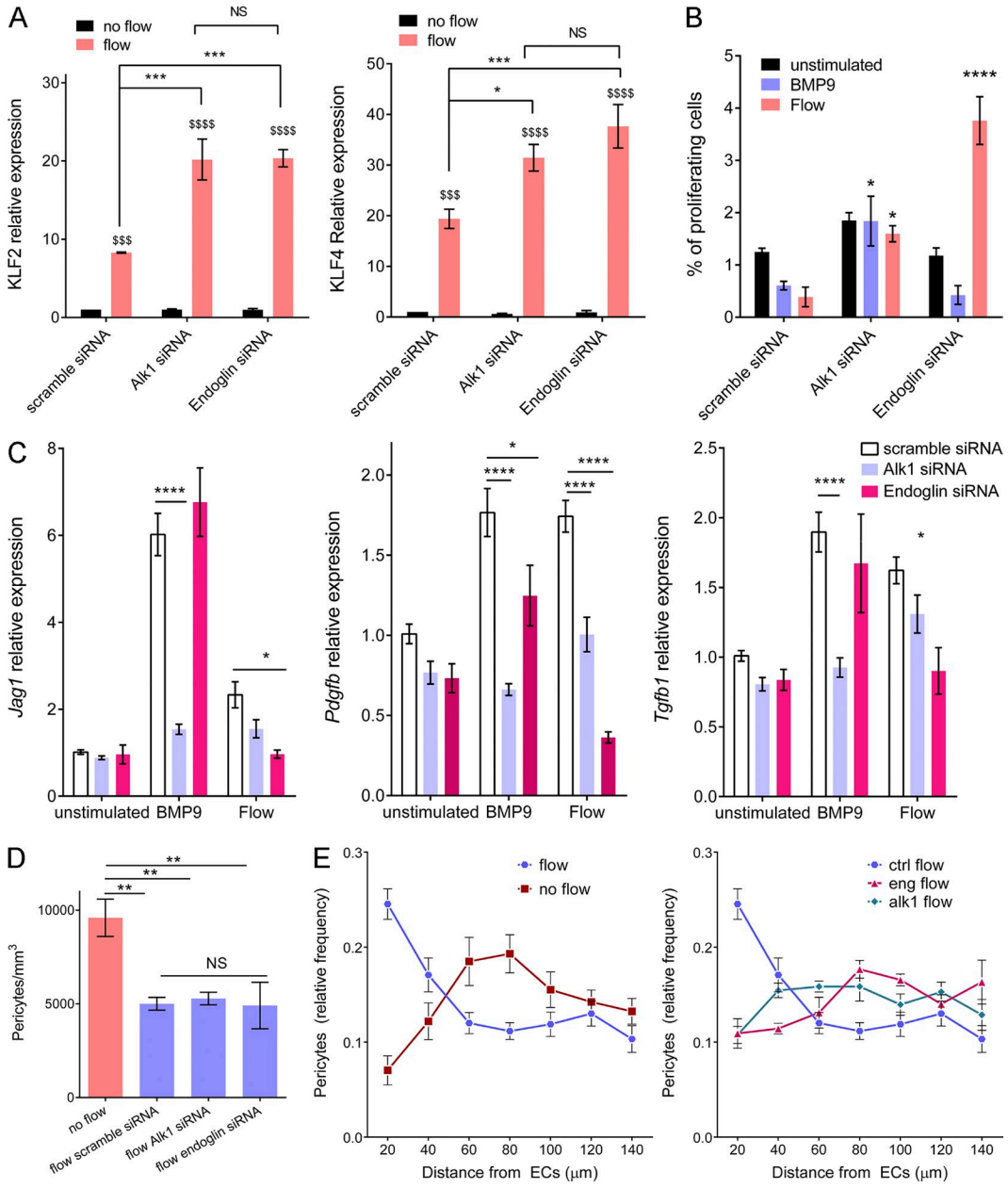

Figure 5. **Effect of Alk1 or endoglin depletion on FSS responses.** (A) KLF2 and KLF4 message levels by quantitative RT-PCR after flow for 16 h in HUV ECs transfected with scrambled, *Alk1*, or *Endoglin* siRNA (QIAGEN; $n = 3$, two-way ANOVA; *, $P < 0.05$; *** or $$$, $P < 0.001$; **** or $$$$, $P < 0.0001$). (B) Endothelial cell proliferation in response to 1 ng/ml BMP9 or 12 dynes/cm^2 for 24 h after transfection with scrambled, *Alk1*, or *Endoglin* siRNA (QIAGEN). Cell proliferation was measured by incorporation of EdU during the last 4 h. (C) HUVECs were stimulated by 1 ng/ml BMP9 or 12 dynes/cm^2 for 3 h. Expression of pericyte recruitment genes (PDGF, TGF-β< and jagged1) was assayed by quantitative RT-PCR ($n = 4$–12, two-way ANOVA; *, $P < 0.05$; **, $P < 0.01$; ****, $P < 0.0001$). (D) Pericyte density in fibrin gels without stimulation or after 96 h of 10 dynes/cm^2 flow on HUVECs transfected with scrambled, *Alk1*, or *Endoglin* siRNA (QIAGEN; $n = 4$–6 gels from four independent experiments, two-way ANOVA; **, $P < 0.01$). (E) Distribution of pericytes in fibrin gels, relative to the endothelial monolayer with or without 10 dynes/cm^2 flow for 96 h. HUVECs were transfected with scrambled, *Alk1*, or *Endoglin* siRNA (QIAGEN); $n = 5$–7 gels from four independent experiments, two-way ANOVA; * or $, $P < 0.05$; **, $P < 0.01$; **** or $$$$, $P < 0.0001$; NS, not significant.

blockade by BMP9 but actively reversed the effect of flow on cell cycle progression; that is, after endoglin knockdown, FSS stimulated instead of inhibited DNA synthesis. When mural cell recruitment genes were assayed, both BMP9 and FSS induced expression of *Pdgfb* (encoding PDGF-B), *Tgfb1* (encoding TGF-β1), and *Jag1* (encoding Jagged1; Fig. 5 C). Alk1 knockdown reduced expression of these genes in response to both flow and BMP9, whereas endoglin knockdown reduced responses to FSS, but not BMP9.

To test the functional relevance of these effects, we established a co-culture system in which endothelial cells were plated on top of fibrin gels containing pericytes. Because fibrin polymerizes over several minutes, the suspended cells settle a short distance, leaving an ∼100-μm gap between the EC layer and the pericytes. Co-cultures were then maintained for 96 h, with or without flow over the EC layer. As a control, we checked for the previously observed inhibition of pericyte proliferation by application of flow to the EC layer (Nackman et al., 1998). FSS

inhibited pericyte proliferation, which was unaffected by Alk1 or endoglin depletion (Fig. 5 D). As expected, FSS enhanced migration of the pericytes toward the endothelial monolayer, which was strongly inhibited by knockdown of either Alk1 or endoglin (Fig. 5 E and Fig. S3). These results demonstrate that, as expected from effects on gene expression, flow stimulation of pericyte recruitment requires the Alk1–endoglin pathway.

The structure and organization of the vascular system is controlled by intricate crosstalk between soluble mediators and physical forces. Integration of information from these various kinds of environmental stimuli controls blood vessel location, diameter, and morphology for optimal tissue perfusion. The current study identifies a specific synergy between blood flow and the BMP9–Alk1–endoglin pathway by which shear stress greatly sensitizes cells to low concentrations of BMP9. This synergy specifically requires endoglin, whereas the response to BMP9 in the absence of flow does not, and correlates with physical association of Alk1 and endoglin. Consistent with a study showing that endoglin extracellular domain binds BMP9 and BMP10 (Castonguay et al., 2011), we hypothesize that association of Alk1 and endoglin could increase binding affinity for BMP ligands to mediate the observed effects.

Telangiectasias and AVMs resulting from HHT are caused mainly by germline heterozygous loss-of-function mutations in *Alk1* or *Endoglin*. A second hit that further suppresses this pathway, perhaps with additional environmental inputs such as inflammation or angiogenesis, leads to clonal expansion, resulting in dilated or expanded vessels with poor mural cell recruitment. The data shown here show that loss of this pathway blocks two key components in flow-induced vascular stabilization: inhibition of EC proliferation and induction of mural cell recruitment. Potentiation of other flow responses, such as increased transcription of KLF2/4, may also contribute. The resultant vessels are therefore dilated and fragile, and readily rupture, which is the major source of morbidity for HHT patients.

BMP9 and BMP10 clearly function in the absence of flow to restrain vascular sprouting, which precedes onset of flow in new vascular beds. Circulating levels of these ligands are high during embryogenesis and drop after birth (Larrivée et al., 2012; Ricard et al., 2012), consistent with decreased sprouting with age. However, even the low levels found in adults should be sufficient to synergize with flow to promote vascular stabilization.

Fluid shear stress blocks EC cell cycle progression through several mediators, including p53, the CDK inhibitor p21, the histone methyltransferase EZH2, and nuclear aryl hydrocarbon receptors (Lin et al., 2000; Han et al., 2008; McDonald et al., 2015; Maleszewska et al., 2016). The current work identifies endoglin and Alk1 as critical components of flow-induced cell cycle blockade, with endoglin as the flow-specific component. These findings may be important in atherosclerosis, where low-flow segments of arteries have high susceptibility to disease, associated with high rates of proliferation, or for other classes of vascular malformations. Importantly, FSS within the physiological range induces vessel quiescence and stabilization, whereas low or high shear promote remodeling (Baeyens and Schwartz, 2016). Smad1 was also specifically activated at physiological shear, with minimal activation below or above that range, strengthening the link to vessel quiescence (Baeyens et al., 2015). The physiological role of this effect is most likely to ensure that only vascular segments that carry the appropriate level of blood flow are stabilized during development or remodeling.

In summary, we report that the Alk1–endoglin complex functions as a joint BMP/flow receptor that governs vascular morphogenesis through regulation of vessel stabilization. Its mutation in HHT results in formation of dilated, fragile vessels prone to rupture. Elucidation of the molecular mechanism by which flow acts on these receptors to enhance BMP signaling may identify new targets for therapy as well as allow us to understand fundamental aspects of vascular mechanotransduction that may be relevant for a wider range of problems.

Materials and methods

Mice

Alk1^{iEC} mice were obtained by crossing *Cdh5-CreERT2* (provided by R. Adams, Max Planck Institute, Muenster, Germany; Wang et al., 2010) and *Alk1flox* (*Alk1*$^{l/l}$) mice (provided by P. Oh, University of Florida, Gainsville, FL; Aspalter et al., 2015). Mice received intraperitoneal injections of 50 µg tamoxifen (T5648, 1 mg/ml; Sigma-Aldrich) at P3 and were killed at P5. Tamoxifen-injected Cre-negative littermates were used as controls. *Alk1*^{iEC} mice were further crossed with the reporter line *Tg(CAG-DsRED-MST)Nagy/J* (*mTmG*; The Jackson Laboratory). 5 µg tamoxifen was injected to induce a mosaic deletion. BMP9/BMP10 blocking antibodies (provided by Genentech, South San Fransisco, CA) at 10 mg/kg were injected intraperitoneally at P3 and P4 and mice sacrificed at P5.

Whole-mount immunostaining

Eyes of P5 pups were fixed in 4% PFA for 20 min at RT. Retinas were dissected; blocked for 1 h at RT in 1% FBS, 3% BSA, 0.5% Triton X-100, and 0.01% sodium deoxycholate in PBS, pH 7.4; and then incubated with phospho–histone PH3 (#06570; EMD Millipore) or NG2 (#Ab5320; EMD Millipore) overnight. Retinas were washed, incubated with isolectin B4 in PBLEC (1 mM $MgCl_2$, 1 mM $CaCl_2$, 0.1 mM $MnCl_2$, and 1% Triton X-100 in PBS) and corresponding secondary antibodies for 1 h at RT, washed, and mounted in fluorescent mounting medium (Dako). Images were acquired using an SP5 confocal microscope (Leica Biosystems) with a spectral detection system (15 SP detector; Leica Biosystems) and the Leica application suite advanced fluorescence software. Quantification of retinal vasculature was done using ImageJ.

Cell culture

HUVECs in which each batch was pooled from three different donors were obtained from the Yale Vascular Biology and Therapeutics program. Cells were cultured in EGM-2 (Lonza) and used between passages 3 and 5. Human dermal microvascular endothelial cells (provided by J. Pober, Yale University, New Haven, CT) were cultured in EGM-2 and used between passages 8 and 9.

siRNA transfections

siRNAs were purchased from QIAGEN (Flexitube siRNA Alk1_5 and Eng_5) and GE Healthcare (ON-TARGET plus Smartpool human *Alk1* and Smartpool human *Endoglin*). The following siRNA sequences were used: *PECAM*, 5′-GGCCCCAAUACACUUCACA-3′ and 5′-AACCACUGCAGAGUACCAG-3′; and *VEGFR2*, 5′-GGG CAUGUACUGACGAUUA-3′ and 5′-CUACAUUGUUCUUCC GAUA-3′. HUVECs were transfected using RNAiMax (Invitrogen) with 100 pmol siRNA per 100-mm plate according to the manufacturer's instructions and used at 48 h.

Adenoviral expression

Human Alk1-GFP or endoglin-GFP were mutated to confer siRNA resistance with a QuikChange site-directed mutagenesis kit (QIAGEN) and cloned into the pEntr1A vector (Invitrogen). Primers used for the mutagenesis were Alk1 forward, 5′-GGGGCGCCCCACCGAATT CGTAAATCACTACTGCTGCGAC-3′; Alk1 reverse, 5′-GTCGCA GCAGTAGTGATTTACGAATTCGGTGGGGCGCCCC-3′; ENG forward, 5′-GTGCCGACGACGCCATGACACTAGTCCTAAAGAAAG AGCTTGTTG-3′; ENG reverse, 5′-CAACAAGCTCTTTCTTTAGGA CTAGTGTCATGGCGTCGTCGGCAC-3′. Inserts were then transferred into pAd/CMV/V5/DEST using the Gateway System (Invitrogen). HEK293 cells were transfected with Pac1-linearized adenoviral constructs using Lipofectamine 2000 (Invitrogen). After 7–10 d, adenovirus-containing supernatant was collected and amplified by reinfection of HEK293 cells. HUVECs were infected with the virus in growth medium overnight and used 48 h later.

Shear stress

Cells were seeded on slides coated with 20 µg/ml fibronectin (2 h at 37°C) and grown to confluence. For short-term experiments, cells were starved in EBM-2 medium containing 0.2% FBS for 4 h. For co-culture, cells were kept in 10% FBS. Shear stress with a calculated intensity of 12 dynes/cm^2 was applied in a parallel flow chamber (Tzima et al., 2005) for the indicated times.

Immunofluorescence

Cells were fixed for 10 min with 3.7% PFA, permeabilized for 10 min with 1% Triton X-100 in PBS, blocked for 30 min with Starting Block blocking buffer (Thermo Fisher Scientific), and probed with primary antibodies overnight. Antibodies used were Smad1 (9743; Cell Signaling Technology), Smad5 (13724; Abcam), Smad8 (ab124094; Abcam), Alk1 (AF370; R&D Systems), and endoglin (AF1097; R&D Systems) or VE-cadherin (sc-6458; Santa Cruz Biotechnology, Inc.). Cells were washed, incubated with secondary antibodies and DAPI for 2 h, washed again, and mounted in Fluoromount G. Images were captured with a 20× objective on a PerkinElmer spinning disk confocal microscope. Image analysis of Smad translocation was performed as described previously (Baeyens et al., 2014).

Western blots

Cells were washed with cold PBS and extracted in Laemmli's buffer. Samples were run on SDS-PAGE gels and transferred onto nitrocellulose membranes. Membranes were blocked with 5% milk and probed with primary antibodies overnight at 4°C: pSmad1,5,8 (13820; Cell Signaling Technology), Smad1 (9743; Cell Signaling Technology), VEGFR2 (9698; Cell Signaling Technology), Alk1 (AF370; R&D Systems), endoglin (AF1097; R&D Systems), and actin (Santa Cruz Biotechnology, Inc.). HRP-conjugated secondary antibodies (Vector Laboratories) were used to detect primary antibodies.

Immunoprecipitation

HUVECs were infected with human Alk1-GFP adenovirus as described in Adenoviral expression. After stimulation, slides were immersed in ice-cold PBS and then extracted at 4°C in 100 mM NaCl, 1 mM $MgCl_2$, 0.5% NP-40, 0.1% sodium deoxycholate, 1.5× Halt protease and phosphatase inhibitor (Thermo Fisher Scientific), and 25 mM Tris, pH 7.4. Lysates were passed through a 25-gauge needle four times and incubated under gentle agitation for 30 min at 4°C. Lysates were centrifuged at 4°C for 10 min (20,000 *g*) and incubated with a GFP-Trap (ChromoTek) for 3 h at 4°C with gentle agitation. Beads were collected by centrifugation, washed three times with 25 mM Tris, pH 7.4, 100 mM NaCl, 1 mM $MgCl_2$, and 0.1% sodium deoxycholate, and extracted in Laemmli sample buffer heated to boiling for 10 min.

RNA isolation and real-time PCR

Total RNA was extracted using RNeasy Plus mini kits (QIAGEN). cDNA synthesis was performed with an iScript cDNA synthesis kit (Bio-Rad Laboratories). Quantitative real-time PCR was performed in triplicate, using an iQSYBR Green Supermix kit and CFX96TM real-time system (Bio-Rad Laboratories). Thermocycling conditions were 95°C for 3 min, followed by 40 cycles that used 95°C for 10 s and 60°C for 30 s. Gene expression was normalized with GAPDH, and relative expression was calculated using the ΔΔCt method. Predesigned primers were obtained from QIAGEN (Quantitect Primer Assay).

Proliferation assay

Cells were stimulated for 20 h with 1 ng/ml BMP9 or 12 dynes/cm^2 for 20 h. EdU (Invitrogen) was added, and cells were incubated for 4 h and then fixed and immunostained for EdU according to the manufacturer's recommendations. Approximately 25,000 cells (100 20× images by slide) were imaged for each condition and analysis of EdU-positive and total nuclei were performed with a custom MATLAB script.

Co-culture

Pericytes (200,000 cells/gel; PromoCell) were suspended in 800 µl fibrinogen at 2.5 mg/ml (Sigma-Aldrich) in EBM-2 supplemented with 1% FBS and 50 µg/ml aprotinin to prevent gel lysis (Sigma-Aldrich). Gels were poured into the wells created by 25-mm circular silicon gaskets on glass slides coated with Parafilm. Fibrin formation was initiated by addition of 1 U thrombin (Sigma-Aldrich). After 30 min at 37°C, HUVECs were plated on top of the fibrin gel for 60 min. The dish was then filled with growth media, cultured overnight, and transferred to starvation medium (10% FBS) for 4 h. Cells were sheared at 10 dynes/cm^2 for 96 h, fixed for 2 h in 3.7% PFA, permeabilized for 15 min with 1% Triton X-100, blocked with Starting Block blocking buffer for 30 min, and probed with DAPI and phalloidin for 4 h under gentle agitation. Coverslips were placed on top of the gels in Fluoromount G and imaged with a 20× objective on a scanning confocal SP5 microscope. Z stacks of 200–250-µm thickness, starting from the endothelial cell layer, were acquired for each gel in 1-µm steps. Pericyte migration was measured by a custom MATLAB script that identified the centroids of cell nuclei for each image acquired in the z stack by normalized pixel intensity and matched them with the centroids of the successive images. Individual nucleus depth was taken as the brightest image in the z stack for each particular centroid relative to the position of the endothelial cells.

Statistical analysis

Data are expressed as means ± SEM. Statistical significance for paired samples and for multiple comparisons was determined by Mann–Whitney and analysis of variance (ANOVA), respectively. Data were considered statistically significant if the p-value was <0.05.

Online supplemental material

Fig. S1 shows the nuclear translocation of Smad1, Smad5, and Smad8 in HUVECs in response to flow or BMP9. It also shows the phosphorylation of Smad1/5/8 in HDMECs as well as the dose response of BMP9 activity in the absence of endoglin and immunoblotting showing the rescue of *Alk1* and *Endoglin* siRNA-treated HUVECs with siRNA-resistant constructs. Fig. S2 shows that NG2-positive pericyte coverage is not changed in the retinas of control Cdh5-CerERT2 mTmG mosaic mice. Fig. S3 shows the distribution of pericytes in a 3D endothelial/pericyte co-culture assay in response to flow, in the

presence or absence of *Alk1* or *endoglin*. Online supplemental material is available at http://www.jcb.org/cgi/content/full/jcb.201603106/DC1.

Acknowledgments

N. Baeyens and M.A. Schwartz would like to thank Kristin A. Gerhold, Gael Genet, and Keiichiro Tanaka for their help during the completion of this project. We thank Genentech, Jordan Pober, Paul Oh, and Ralf Adams for generously providing reagents.

This work was funded by an American Heart Association postdoctoral fellowship (14POST19020010, Wallania Brussels International, to N. Baeyens), a World Excellence scholarship (to N. Baeyens), a Belgian American Educational Foundation postdoctoral fellowship (to N. Baeyens), an R0 American Heart Association postdoctoral fellowship (15POST25560114, to A. Dubrac), an American Heart Association postdoctoral fellowship (14POST20380207, to A. Dubrac), National Institutes of Health grant (5T32HL007950, to B.G. Coon), American Heart Association postdoctoral fellowship (13POST16720007, to B.G. Coon), National Heart, Lung, and Blood Institute grants (1R01EY025979 and 1R01HL125811, to A. Eichmann), and U.S. Public Health Service grant (PO1 HL107205, to M.A. Schwartz).

The authors declare no competing financial interests.

Author contributions: N. Baeyens and B. Larrivée originated the project, designed experiments, acquired and analyzed data, and drafted the manuscript. R. Ola and A. Dubrac acquired and analyzed mouse data. B. Hayward-Piatkowskyi performed the immunoprecipitation experiment. B. Huang and T.D. Ross developed analytical tools for image analysis and analyzed the data (B. Huang: pericyte recruitment; T.D. Ross: EdU incorporation). B.G. Coon contributed to experimental design and data analysis. M. Tsarfati and E. Min acquired data. H. Tong contributed to adenovirus production. A. Eichmann and M. Schwartz provided direct supervision and intellectual insight necessary for project completion, experimental design, data analysis, and manuscript drafting.

Submitted: 30 March 2016
Accepted: 30 August 2016

References

Akimoto, S., M. Mitsumata, T. Sasaguri, and Y. Yoshida. 2000. Laminar shear stress inhibits vascular endothelial cell proliferation by inducing cyclin-dependent kinase inhibitor p21(Sdi1/Cip1/Waf1). *Circ. Res.* 86:185–190. http://dx.doi.org/10.1161/01.RES.86.2.185

Arthur, H.M., J. Ure, A.J. Smith, G. Renforth, D.I. Wilson, E. Torsney, R. Charlton, D.V. Parums, T. Jowett, D.A. Marchuk, et al. 2000. Endoglin, an ancillary TGFbeta receptor, is required for extraembryonic angiogenesis and plays a key role in heart development. *Dev. Biol.* 217:42–53. http://dx.doi.org/10.1006/dbio.1999.9534

Aspalter, I.M., E. Gordon, A. Dubrac, A. Ragab, J. Narloch, P. Vizán, I. Geudens, R.T. Collins, C.A. Franco, C.L. Abrahams, et al. 2015. Alk1 and Alk5 inhibition by Nrp1 controls vascular sprouting downstream of Notch. *Nat. Commun.* 6:7264. http://dx.doi.org/10.1038/ncomms8264

Atri, D., B. Larrivee, A. Eichmann, and M. Simons. 2014. Endothelial signaling and the molecular basis of arteriovenous malformation. *Cell. Mol. Life Sci.* 71:867–883. http://dx.doi.org/10.1007/s00018-013-1475-1

Baeyens, N., and M.A. Schwartz. 2016. Biomechanics of vascular mechanosensation and remodeling. *Mol. Biol. Cell.* 27:7–11. http://dx.doi.org/10.1091/mbc.E14-11-1522

Baeyens, N., M.J. Mulligan-Kehoe, F. Corti, D.D. Simon, T.D. Ross, J.M. Rhodes, T.Z. Wang, C.O. Mejean, M. Simons, J. Humphrey, and M.A. Schwartz. 2014. Syndecan 4 is required for endothelial alignment in flow and atheroprotective signaling. *Proc. Natl. Acad. Sci. USA.* 111:17308–17313. http://dx.doi.org/10.1073/pnas.1413725111

Baeyens, N., S. Nicoli, B.G. Coon, T.D. Ross, K. Van den Dries, J. Han, H.M. Lauridsen, C.O. Mejean, A. Eichmann, J.L. Thomas, et al. 2015. Vascular remodeling is governed by a VEGFR3-dependent fluid shear stress set point. *eLife.* 4: e04645. http://dx.doi.org/10.7554/eLife.04645

Bernabeu, M.O., M.L. Jones, J.H. Nielsen, T. Krüger, R.W. Nash, D. Groen, S. Schmieschek, J. Hetherington, H. Gerhardt, C.A. Franco, and P.V. Coveney. 2014. Computer simulations reveal complex distribution of haemodynamic forces in a mouse retina model of angiogenesis. *J. R. Soc. Interface.* 11:20140543. http://dx.doi.org/10.1098/rsif.2014.0543

Castonguay, R., E.D. Werner, R.G. Matthews, E. Presman, A.W. Mulivor, N. Solban, D. Sako, R.S. Pearsall, K.W. Underwood, J. Seehra, et al. 2011. Soluble endoglin specifically binds bone morphogenetic proteins 9 and 10 via its orphan domain, inhibits blood vessel formation, and suppresses tumor growth. *J. Biol. Chem.* 286:30034–30046. http://dx.doi.org/10.1074/jbc.M111.260133

Coon, B.G., N. Baeyens, J. Han, M. Budatha, T.D. Ross, J.S. Fang, S. Yun, J.L. Thomas, and M.A. Schwartz. 2015. Intramembrane binding of VE-cadherin to VEGFR2 and VEGFR3 assembles the endothelial mechanosensory complex. *J. Cell Biol.* 208:975–986. http://dx.doi.org/10.1083/jcb.201408103

Corti, P., S. Young, C.Y. Chen, M.J. Patrick, E.R. Rochon, K. Pekkan, and B.L. Roman. 2011. Interaction between alk1 and blood flow in the development of arteriovenous malformations. *Development.* 138:1573–1582. http://dx.doi.org/10.1242/dev.060467

David, L., C. Mallet, S. Mazerbourg, J.J. Feige, and S. Bailly. 2007. Identification of BMP9 and BMP10 as functional activators of the orphan activin receptor-like kinase 1 (ALK1) in endothelial cells. *Blood.* 109:1953–1961. http://dx.doi.org/10.1182/blood-2006-07-034124

David, L., C. Mallet, M. Keramidas, N. Lamandé, J.M. Gasc, S. Dupuis-Girod, H. Plauchu, J.J. Feige, and S. Bailly. 2008. Bone morphogenetic protein-9 is a circulating vascular quiescence factor. *Circ. Res.* 102:914–922. http://dx.doi.org/10.1161/CIRCRESAHA.107.165530

Dekker, R.J., S. van Soest, R.D. Fontijn, S. Salamanca, P.G. de Groot, E. VanBavel, H. Pannekoek, and A.J. Horrevoets. 2002. Prolonged fluid shear stress induces a distinct set of endothelial cell genes, most specifically lung Krüppel-like factor (KLF2). *Blood.* 100:1689–1698. http://dx.doi.org/10.1182/blood-2002-01-0046

Garrido-Martin, E.M., H.L. Nguyen, T.A. Cunningham, S.W. Choe, Z. Jiang, H.M. Arthur, Y.J. Lee, and S.P. Oh. 2014. Common and distinctive pathogenetic features of arteriovenous malformations in hereditary hemorrhagic telangiectasia 1 and hereditary hemorrhagic telangiectasia 2 animal models--brief report. *Arterioscler. Thromb. Vasc. Biol.* 34:2232–2236. http://dx.doi.org/10.1161/ATVBAHA.114.303984

Hamik, A., Z. Lin, A. Kumar, M. Balcells, S. Sinha, J. Katz, M.W. Feinberg, R.E. Gerzsten, E.R. Edelman, and M.K. Jain. 2007. Kruppel-like factor 4 regulates endothelial inflammation. *J. Biol. Chem.* 282:13769–13779. http://dx.doi.org/10.1074/jbc.M700078200

Han, Z., Y. Miwa, H. Obikane, M. Mitsumata, F. Takahashi-Yanaga, S. Morimoto, and T. Sasaguri. 2008. Aryl hydrocarbon receptor mediates laminar fluid shear stress-induced CYP1A1 activation and cell cycle arrest in vascular endothelial cells. *Cardiovasc. Res.* 77:809–818. http://dx.doi.org/10.1093/cvr/cvm095

Larrivée, B., C. Prahst, E. Gordon, R. del Toro, T. Mathivet, A. Duarte, M. Simons, and A. Eichmann. 2012. ALK1 signaling inhibits angiogenesis by cooperating with the Notch pathway. *Dev. Cell.* 22:489–500. http://dx.doi.org/10.1016/j.devcel.2012.02.005

Laux, D.W., S. Young, J.P. Donovan, C.J. Mansfield, P.D. Upton, and B.L. Roman. 2013. Circulating Bmp10 acts through endothelial Alk1 to mediate flow-dependent arterial quiescence. *Development.* 140:3403–3412. http://dx.doi.org/10.1242/dev.095307

Lin, K., P.P. Hsu, B.P. Chen, S. Yuan, S. Usami, J.Y. Shyy, Y.S. Li, and S. Chien. 2000. Molecular mechanism of endothelial growth arrest by laminar shear stress. *Proc. Natl. Acad. Sci. USA.* 97:9385–9389. http://dx.doi.org/10.1073/pnas.170282597

Maleszewska, M., B. Vanchin, M.C. Harmsen, and G. Krenning. 2016. The decrease in histone methyltransferase EZH2 in response to fluid shear stress alters endothelial gene expression and promotes quiescence. *Angiogenesis.* 19:9–24. http://dx.doi.org/10.1007/s10456-015-9485-2

McDonald, J., W. Wooderchak-Donahue, C. VanSant Webb, K. Whitehead, D.A. Stevenson, and P. Bayrak-Toydemir. 2015. Hereditary hemorrhagic telangiectasia: genetics and molecular diagnostics in a new era. *Front. Genet.* 6:1. http://dx.doi.org/10.3389/fgene.2015.00001

Nackman, G.B., M.F. Fillinger, R. Shafritz, T. Wei, and A.M. Graham. 1998. Flow modulates endothelial regulation of smooth muscle cell proliferation: a new model. *Surgery.* 124:353–361. http://dx.doi.org/10.1016/S0039-6060(98)70141-2

Oh, S.P., T. Seki, K.A. Goss, T. Imamura, Y. Yi, P.K. Donahoe, L. Li, K. Miyazono, P. ten Dijke, S. Kim, and E. Li. 2000. Activin receptor-like

kinase 1 modulates transforming growth factor-beta 1 signaling in the regulation of angiogenesis. *Proc. Natl. Acad. Sci. USA*. 97:2626–2631. http://dx.doi.org/10.1073/pnas.97.6.2626

Park, S.O., M. Wankhede, Y.J. Lee, E.J. Choi, N. Fliess, S.W. Choe, S.H. Oh, G. Walter, M.K. Raizada, B.S. Sorg, and S.P. Oh. 2009. Real-time imaging of de novo arteriovenous malformation in a mouse model of hereditary hemorrhagic telangiectasia. *J. Clin. Invest.* 119:3487–3496. http://dx.doi.org/10.1172/JCI39482

Ricard, N., D. Ciais, S. Levet, M. Subileau, C. Mallet, T.A. Zimmers, S.J. Lee, M. Bidart, J.J. Feige, and S. Bailly. 2012. BMP9 and BMP10 are critical for postnatal retinal vascular remodeling. *Blood.* 119:6162–6171. http://dx.doi.org/10.1182/blood-2012-01-407593

Shovlin, C.L. 2010. Hereditary haemorrhagic telangiectasia: pathophysiology, diagnosis and treatment. *Blood Rev.* 24:203–219. http://dx.doi.org/10.1016/j.blre.2010.07.001

Sorensen, L.K., B.S. Brooke, D.Y. Li, and L.D. Urness. 2003. Loss of distinct arterial and venous boundaries in mice lacking endoglin, a vascular-specific TGFbeta coreceptor. *Dev. Biol.* 261:235–250. http://dx.doi.org/10.1016/S0012-1606(03)00158-1

Tillet, E., and S. Bailly. 2015. Emerging roles of BMP9 and BMP10 in hereditary hemorrhagic telangiectasia. *Front. Genet.* 5:456. http://dx.doi.org/10.3389/fgene.2014.00456

Tual-Chalot, S., M. Mahmoud, K.R. Allinson, R.E. Redgrave, Z. Zhai, S.P. Oh, M. Fruttiger, and H.M. Arthur. 2014. Endothelial depletion of Acvrl1 in mice leads to arteriovenous malformations associated with reduced endoglin expression. *PLoS One.* 9:e98646. http://dx.doi.org/10.1371/journal.pone.0098646

Tual-Chalot, S., S.P. Oh, and H.M. Arthur. 2015. Mouse models of hereditary hemorrhagic telangiectasia: recent advances and future challenges. *Front. Genet.* 6:25. http://dx.doi.org/10.3389/fgene.2015.00025

Tzima, E., M. Irani-Tehrani, W.B. Kiosses, E. Dejana, D.A. Schultz, B. Engelhardt, G. Cao, H. DeLisser, and M.A. Schwartz. 2005. A mechanosensory complex that mediates the endothelial cell response to fluid shear stress. *Nature.* 437:426–431. http://dx.doi.org/10.1038/nature03952

Van Gieson, E.J., W.L. Murfee, T.C. Skalak, and R.J. Price. 2003. Enhanced smooth muscle cell coverage of microvessels exposed to increased hemodynamic stresses in vivo. *Circ. Res.* 92:929–936. http://dx.doi.org/10.1161/01.RES.0000068377.01063.79

Wang, Y., M. Nakayama, M.E. Pitulescu, T.S. Schmidt, M.L. Bochenek, A. Sakakibara, S. Adams, A. Davy, U. Deutsch, U. Lüthi, et al. 2010. Ephrin-B2 controls VEGF-induced angiogenesis and lymphangiogenesis. *Nature*. 465:483–486. http://dx.doi.org/10.1038/nature09002

Zhou, J., P.L. Lee, C.S. Tsai, C.I. Lee, T.L. Yang, H.S. Chuang, W.W. Lin, T.E. Lin, S.H. Lim, S.Y. Wei, et al. 2012. Force-specific activation of Smad1/5 regulates vascular endothelial cell cycle progression in response to disturbed flow. *Proc. Natl. Acad. Sci. USA.* 109:7770–7775. (published erratum appears in *Proc. Natl. Acad. Sci. U S A.* 2012. 109:14716) http://dx.doi.org/10.1073/pnas.1205476109